Nuclear Engineering and Design 49 (1978) 155–173

ANALYSIS AND APPLICATION OF PRESTRESSED CONCRETE REACTOR VESSELS FOR LMFBR CONTAINMENT

A.H. MARCHERTAS, S.H. FISTEDIS
Engineering Mechanics Program, Reactor Analysis and Safety Division, Argonne National Laboratory, Argonne, Illinois, USA

Z.P. BAŽANT and T.B. BELYTSCHKO
Department of Civil Engineering, Northwestern University, Evanston, Illinois 60201, USA

An analytical model of a prestressed concrete reactor vessel (PCRV) for LMFBR and the associated finite element computer code, involving an explicit time integration procedure, is described. The model is axisymmetric and includes simulations of the tensile cracking of concrete, the reinforcement, and a prestressing capability. The tensile cracking of concrete and the steel reinforcement are both modeled as continuously distributed within the finite element. The stresses in the reinforcement and concrete are computed separately and combined to give an overall stress state of the composite material. The reinformcement is assumed to be elastic, perfectly-plastic; the concrete is taken to be elastic, with tensile and compressive stress limits. Cracking of concrete is based on the criterion of maximum principal stress; a crack is assumed to form normal to the direction of the maximum principal stress. Attention is also given to the fact that cracks do not form instantaneously, but develop gradually. Thus, after crack initiation the normal stress is reduced to zero gradually as a function of time. Residual shear resistance of cracks due to aggregate interlock is also taken into account. An existing crack is permitted to close. Prestressing of the PCRV is modeled by special structural members which represent an averaged prestressing layer equivalent to an axisymmetric shell. The internal prestressing members are superimposed over the reinforced concrete body of the PCRV; they are permitted to stretch and slide in a predetermined path, simulating the actual tendons.

The validity of the code is examined by comparison with experimental data. Both static and dynamic data are compared with code predictions, and the agreement is satisfactory. A preliminary design has been developed for both pool and loop-type PCRVs. The code was applied to the analysis of these designs. This analysis reveals that the critical locations in such a design would be the head cover and the junction between the cover and the vessel wall and indicates the pattern of crack development. The results show that the development of a design adequate for current HCDA loads is quite feasible for pool-type or loop-type PCRVs.

1. Introduction

Prestressed concrete vessels (PCRVs), have recently received keen attention as a means of improving the capability of sustaining hypothetical core disruptive accidents (HCDAs) in a liquid metal fast breeder reactor (LMFBR). This concept, in which the PCRV serves as a secondary vessel and the main energy absorption barrier (originally suggested in ref. [1], takes advantage of the well known favorable characteristics of the PCRV [2].

One favorable characteristic of PCRVs is the absence of brittle failure on the macroscopic scale. In the pressure–deflection curve of a PCRV, the linear elastic response is followed by a long, almost horizontal region at peak load, so the overall behavior is quite ductile. An abrupt decrease of load-carrying ability, i.e. brittle behavior, is never encountered in PCRVs. This advantageous property endows the PCRV with great energy-absorption capability. The ductile behavior of prestressed reinforced concrete derives partly from the micro-inhomogeneity of the material and partly from the cracking behavior of prestressed concrete. Cracks in concrete consist of a system of distributed microcracks rather than isolated cracks with well-defined crack tips characterized by an isolated stress singularity; thus, they do not have a tendency to propagate, and it is very unlikely that a crack would propagate from the area of one prestressing tendon to another.

Other favorable characteristics of PCRV are its great mass, which assists in resisting impact loads; its ability to function as a biological radiation shield as well as a structural member; and its use of relatively inexpensive

high strength steel in the form of cold drawn wire. In view of the preceding, it seems likely that the PCRV may offer economic advantages. The relative economy of the PCRV would grow with increasing size of the vessel, and while the cost of the steel vessel per unit volume grows with the wall thickness, the cost of the PCRV per unit volume decreases with growing wall thickness. So, regardless of the exact unit prices of the material, for a sufficiently large reactor the PCRV will be more economical than a steel vessel, although whether this size is within the probable range of 1000–1500 MW(e) which is currently of interest, remains a question.

For these reasons a research program has been initiated at Argonne National Laboratory to investigate the PCRV application in LMFBRs, and in particular, to examine the response of the PCRV to HCDA loads. The program consists of three phases: (1) investigation of the dynamic response of the vessel to pressures generated in an HCDA; (2) investigation of the response of the concrete vessel to rapid heating, post-accident heat removal and the effect of chemical interactions between liquid sodium and concrete; and (3) study of the design aspects and related questions. This last phase will also include a study of a novel design concept, i.e. the hot-dried concrete vessel which has recently been proposed [3] to improve the performance at high temperatures as well as to ameliorate the effects of possible contact with liquid sodium. The improvement is to be achieved by depriving the concrete of all evaporable water and keeping it hot during reactor operation.

This paper presents the results of an investigation of the dynamic PCRV response as well as its typical designs. It contains an extension of the work described in condensed form in the transactions of a recent conference [4]. In the interest of comprehensive presentation, relevant subject matter from ref. [4] is described here in a more detailed form. Further results are also included, consisting of comparisons of calculations with test data, refinement of the model for cracking, and development of the general PCRV designs for LMFBR and their dynamic analysis.

2. Basic analytical approach

The analysis of the effects of HCDA can be decoupled into two distinct stages: (1) analysis of the propagation of the pressure pulse on the interior wall of PCRV, and (2) analysis of PCRV itself. The two stages can be considered independent of each other because the PCRV is so stiff that it can be treated as a rigid body for purposes of the hydrodynamic analysis of the HCDA. This decoupling not only simplifies the analysis, but also yields a considerable saving of computer time.

The first stage of analysis can be carried out with existing computer codes such as REXCO [5], which uses an explicit Lagrangian time step algorithm, or ICECO [6,7], which uses an implicit Eulerian algorithm. These codes, having been designed for the dynamic evaluations of the LMFBR primary containment subjected to the HCDA loads, are perfectly suited for the present purpose. The combination of finite difference representation of fluid as well as solid structures within the REXCO code enables a fairly detailed representation of the reactor internals. The combination of an explicit time integration feature and Lagrangian hydrodynamic formulation make the code quite efficient. The code can thus analytically model the propagation of pressures from the reactor core to the inside boundaries of the PCRV. This pressure history can then be used as the given loading in a separate analysis of the PCRV vessel.

The second stage of the PCRV containment treatment involves the PCRV analysis, subject to the loading history obtained in the first stage. This part of the overall treatment is not as yet well established. A preliminary computer code which has been developed for transient analysis is described in the following section.

3. Particular features of the analytical model

The PCRV is idealized as an axisymmetric structure. Since the loading is expected to be impulsive and of short duration, the use of an explicit step-by-step integration in time is appropriate. Therefore, the basic framework of the finite element computer code WHAM [8] has been selected. This parent code has been supplemented by a material law that models cracking and reinforcement distributed within a continuum finite element. In an explicit finite element program, the material properties are used exclusively to calculate stress increments from strain increments, and the in-

plementation of constitutive equations must be arranged accordingly. A prestressing capability is also provided. However, more complicated and less important features of the response of the vessel, such as bond slip, dowel action, strain rate sensitivity of concrete, and nonlinearity of concrete under compressive stresses, are relegated to subsequent studies.

3.1. Model for concrete

In the simplified formulation used in this initial stage, a linear elastic representation of the material behavior with tensile and compressive limits is assumed. In compression the concrete is assumed to be able to sustain stresses up to the uniaxial compressive strength f'_c. In tension, cracks are assumed to form when the tensile stress in concrete reaches the uniaxial tensile limit f'_t (fig. 1). As long as no cracks are present within a given element, a triaxial state of stress is assumed. With the existence of one fully developed crack within an element, a state of plane stress is used for the calculations of stress in that element; similarly, with two fully developed cracks present, a uniaxial state of stress is assumed. Finally, with the formation of three cracks, the element is assumed to lose all of its load-carrying capacity and the stresses are set to zero.

For the overall behavior of the vessel this seems to be a reasonable simplification because under internal pressure virtually the entire PCRV is subjected to tensile stress, so the tensile cracking appears to be the most important aspect of the nonlinear behavior of concrete. Thus, emphasis should be placed on simulating crack development.

In conventional models for cracking, the cracks are assumed to form instantaneously. In reality, however, densely reinforced concrete cracks gradually. The gradual crack development is even more true in rapid loading because the coalescence of microcracks into large isolated cracks requires a certain duration which may well be larger than the time step used. Hence, larger cracks may not be able to form during a single time step. Furthermore, if instantaneous formation of cracks is permitted, severely distorted results are obtained because the sudden large stress drop causes spurious elastic waves which cause spurious cracks in adjacent elements; these in turn cause additional waves and this chain reaction soon causes disintegration of the whole structure. If the delay of crack formation is taken into account, cracking is usually more gradual.

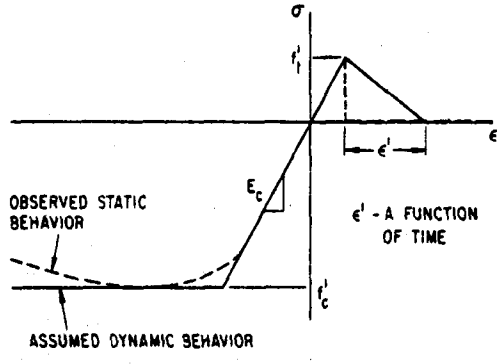

Fig. 1. Idealization of concrete behavior.

For these reasons the formation of a crack is not modeled by an instantaneous reduction of the normal stress to zero; instead, the normal stress is reduced to zero linearly over a prescribed characteristic time period τ, related to ϵ' in fig. 1. Although no sound direct physical estimate of the constant τ is available at present, its physical motivation is clear: the limited rate of crack growth and the energy dissipation in the crack areas found in real concrete.

The initiation of cracking within an element is based on the maximum principal stress criterion. In an axisymmetric (r, z, θ) geometry, the circumferential direction always provides a principal stress. The remaining two principal planes lie within the r–z plane and are given by

$$\left.\begin{matrix}\sigma_{nn}\\ \sigma_{tt}\end{matrix}\right\} = \frac{\sigma_{rr}+\sigma_{zz}}{2} \pm \sqrt{\left(\frac{\sigma_{rr}-\sigma_{zz}}{2}\right)^2 + \sigma_{rz}^2}\,, \qquad (1)$$

where σ_{rr}, σ_{zz}, σ_{rz} are the radial, axial and shear stresses of the r–z plane; σ_{nn} and σ_{tt} are the stresses normal and tangential to an impending crack. When a principal stress exceeds the tensile limit, a crack is considered to be initiated. The direction of the normal to an initiated crack with respect to the r-axis is given by

$$\alpha = \tfrac{1}{2}\arctan[2\sigma_{rz}/(\sigma_{rr}-\sigma_{zz})]\,.$$

Once a crack has been initiated its direction is kept as a permanent record so that the stress or strain normal or tangent to the crack can be monitored during subsequent time steps. The normal, tangential, and shear

strains (ϵ_{nn}, ϵ_{tt}, γ_{nt}) with respect to the crack are,

$$\begin{Bmatrix}\epsilon_{nn}\\ \epsilon_{tt}\\ \gamma_{nt}\end{Bmatrix} = \begin{bmatrix}\cos^2\alpha & \sin^2\alpha & \frac{1}{2}\sin 2\alpha\\ \sin^2\alpha & \cos^2\alpha & -\frac{1}{2}\sin 2\alpha\\ -\sin 2\alpha & \sin 2\alpha & \cos 2\alpha\end{bmatrix}\begin{Bmatrix}\epsilon_{rr}\\ \epsilon_{zz}\\ \gamma_{rz}\end{Bmatrix}, \quad (2)$$

where ϵ_{rr}, ϵ_{zz}, γ_{rz} are the engineering (small) normal strains in the radial, axial directions, and shear angle in the r–z plane, respectively.

The strains of eqs. (2) within a given element are related to the stresses as follows:

$$\begin{Bmatrix}\sigma_{nn}\\ \sigma_{tt}\\ \sigma_{nt}\\ \sigma_{\theta\theta}\end{Bmatrix} = E_1\begin{bmatrix}1 & \nu_1 & 0 & \nu_1\\ \nu_1 & 1 & 0 & \nu_1\\ 0 & 0 & G & 0\\ \nu_1 & \nu_1 & 0 & 1\end{bmatrix}\begin{Bmatrix}\epsilon_{nn}\\ \epsilon_{tt}\\ \epsilon_{nt}\\ \epsilon_{\theta\theta}\end{Bmatrix}, \quad (3)$$

where $\nu_1 = \nu/(1-\nu)$, $E_1 = 2G(1-\nu)/(1-2\nu)$, E is Young's modulus of elasticity, ν is Poisson's ratio, and G is the shear modulus.

Eqs. (3) are also used for the case where cracking is assumed to have initiated, but a definite crack opening is not as yet present. Such a state is assumed to be possible in the presence of microcracks in brittle materials [9]. For purposes of illustrating the crack initiation model, the principal stresses of eq. (3) are arranged so that $\sigma_1 > \sigma_2 > \sigma_3$. Initially σ_1 will be equal to σ_{nn} or $\sigma_{\theta\theta}$ depending on which one is of greater magnitude. Since cracking is based on the maximum principal stress, crack initiation should first occur normal to σ_1. Once the principal stress σ_1 reaches or exceeds the tensile limit f'_t, the stress normal to the impending crack is prescribed and is usually independent of the strain normal to the crack. At the instant when the maximum uniaxial tensile limit is reached or exceeded by the principal stress, the stress normal to the impending crack is set equal to the tensile limit f'_t. During the subsequent time increments the tensile stress normal to the impending crack is degraded by equal decrements, as follows:

$$\sigma_1 = f'_t\left(1 - \frac{t}{\tau}\right) \qquad (\sigma_1 > 0), \quad (4)$$

where t is the time elapsed from crack initiation and τ is the decay constant, as shown in fig. 2. This equation applies as long as the σ_1 is positive; if $\sigma_1 \geqslant 0$, then the formation of a crack is considered completed; a fully

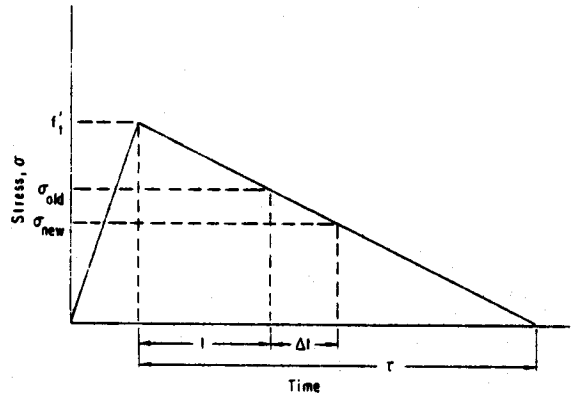

Fig. 2. History of crack formation.

developed crack is assumed to have occurred.

It should be noted that if any of the principal stresses are prescribed, the other principal stresses are affected correspondingly. For example, if the prescribed stress across the crack is taken to be σ_A, the strain component ϵ_{nn} in eq. (3) is solved for and substituted into the expressions of the other principal stresses. The state of stress in the element becomes

$$\sigma_1^* = \sigma_A\,; \qquad \sigma_2^* = \sigma_2 + \nu_1(\sigma_A - \sigma_1)\,,$$

$$\sigma_3^* = \sigma_3 + \nu_1(\sigma_A - \sigma_1)\,; \qquad \sigma_{nt}^* = G\gamma_{nt}\,.$$

Similarly, if two principal stresses σ_A, σ_B are prescribed the element state of stress becomes

$$\sigma_1^* = \sigma_A\,; \qquad \sigma_2^* = \sigma_B\,,$$

$$\sigma_3^* = E\epsilon_3 + \nu(\sigma_A + \sigma_B)\,; \qquad \sigma_{nt}^* = G\gamma_{nt}\,,$$

where ϵ_3 is the minimum principal strain. Finally, if all three principal stresses are prescribed, σ_A, σ_B, σ_C, then the state of stress becomes

$$\sigma_1^* = \sigma_A\,; \qquad \sigma_2^* = \sigma_B\,,$$

$$\sigma_3^* = \sigma_C\,; \qquad \sigma_{nt}^* = G\gamma_{nt}\,.$$

Note that the prescribed stresses σ_A, σ_B, σ_C need not be equal. This may occur, for example, if a second or third crack form in an element. As long as no fully developed cracks exist, concurrent crack development is assumed to originate in orthogonal directions.

It may be noted that a more realistic way to model progressive tensile cracking would be to take into account the nonlinearity of tensile stress–strain behavior and tensile strain-softening, which would entail a nonlinear tensile stress–strain relationship. This rela-

tionship must exhibit the elastic anisotropy introduced by partial cracking in particular directions. To express this in a tensorially invariant form, it would be necessary to postulate a damage tensor the components of which describe the reduction of elastic stiffness in various directions.

The transformation of principal stresses to stresses in cylindrical coordinates (r, z, θ) must also be provided for. Since θ is the principal coordinate, no change is necessary for the circumferential stress $\sigma_{\theta\theta}$. The stress components in the r–z plane, however, require the following transformation:

$$\begin{Bmatrix} \sigma_{rr} \\ \sigma_{zz} \\ \sigma_{rz} \end{Bmatrix} = \begin{bmatrix} \cos^2\alpha & \sin^2\alpha & -\sin 2\alpha \\ \sin^2\alpha & \cos^2\alpha & \sin 2\alpha \\ \frac{1}{2}\sin 2\alpha & -\frac{1}{2}\sin 2\alpha & \cos 2\alpha \end{bmatrix} \begin{Bmatrix} \sigma^*_{nn} \\ \sigma^*_{tt} \\ \sigma^*_{nt} \end{Bmatrix}. \quad (5)$$

The state of stress in an element with one fully developed radial crack is established by the previous equations provided that $\sigma_{\theta\theta}$ is set to zero. However, with a fully developed crack in the r–z plane the presence of aggregate interlock makes the conditions somewhat more complicated. It has been suggested [10] that the effect of aggregate interlock can be accounted for by a shear reduction term as follows:

$$\begin{Bmatrix} \sigma_{tt} \\ \sigma_{nt} \\ \sigma_{\theta\theta} \end{Bmatrix} = \frac{E}{1-\nu^2} \begin{bmatrix} 1 & 0 & \nu \\ 0 & \beta G & 0 \\ \nu & 0 & 1 \end{bmatrix} \begin{Bmatrix} \epsilon_{tt} \\ \epsilon_{nt} \\ \epsilon_{\theta\theta} \end{Bmatrix}, \quad (6)$$

where β is the shear reduction factor, a constant usually taken as 0.5. This means that the shear strain tangent to the crack is assumed to be reduced by the factor β from what it would be in the absence of a crack. Although a constant factor for any crack size and aggregate surface is a rather rough estimate, it seems to yield fairly good results under static conditions. Lacking any better means of accounting for aggregate interlock, the same approach is retained in this formulation.

Because of the existence of the shear stress due to aggreate interlock, the perpendicular to the normal of the existing crack within an element is not a principal direction. The second principal stress in the r–z plane, which is used to check for secondary cracks, and the angle of its normal with respect to the r-axis are

$$\sigma^*_{tt} = \tfrac{1}{2}\sigma_{tt} + \sqrt{(\tfrac{1}{2}\sigma_{tt})^2 + \sigma^2_{nt}},$$
$$\alpha^* = \alpha + \tfrac{1}{2}\arctan(-2\sigma_{nt}/\sigma_{tt}). \quad (7)$$

The non-orthogonal cracking in the r–z plane causes another complication. With one crack fully developed and another impending, there are a total of four stress values to be prescribed but the stress tensor has only three independent components. This difficulty is resolved in the following manner: the normal stresses across the two cracks are given by eq. (4) and the shear stress σ_{nt} of the first crack is computed by the shear reduction factor β, as described before. The shear stress σ^*_{nt} along the impending crack, however, is obtained from equilibrium considerations, as shown in fig. 3. Moment equilibrium shows that the shear stresses tangent to the new crack is given by

$$\sigma^*_{nt} = \sigma_{nt} + \sigma^*_{tt}\tan(\alpha^* - \alpha). \quad (8)$$

From force equilibrium the following expressions are obtained:

$$\begin{Bmatrix} \sigma_{rr} \\ \sigma_{zz} \\ \sigma_{rz} \end{Bmatrix} = \frac{1}{\cos^2(\alpha-\alpha^*)} \begin{bmatrix} \sin\alpha\sin(2\alpha^*-\alpha) & -2\sin\alpha\cos\alpha^*\cos(\alpha-\alpha^*) \\ \cos\alpha\cos(2\alpha^*-\alpha) & 2\sin\alpha^*\cos\alpha\cos(\alpha-\alpha^*) \\ -\frac{1}{2}\sin 2\alpha^* & \frac{1}{2}(\cos 2\alpha^* + \cos 2\alpha) \end{bmatrix} \times \begin{Bmatrix} \sigma^*_{tt} \\ \sigma^*_{nt} \end{Bmatrix}. \quad (9)$$

It may be observed that eq. (9) reduces to eq. (5) provided that σ_{nn} is set to zero and α^* is set equal to α. Eq. (9) pertains to the case where the second crack in the r–z plane is in the process of formation, or has been fully developed. Thus, $\sigma^*_{tt} = f'_t$ if the second crack is at the instant of being formed, $\sigma^*_{tt} = \sigma_1$ [see eq. (4)] during crack formation, and $\sigma^*_{tt} = 0$ if the crack is fully formed.

After the second crack in the r–z plane has fully developed and σ^*_{tt} is set to zero, the remaining stresses are calculated by

$$\begin{Bmatrix} \sigma_{nt} \\ \sigma_{\theta\theta} \end{Bmatrix} = E \begin{bmatrix} 0 & 1 \\ \beta G & 0 \end{bmatrix} \begin{Bmatrix} \epsilon_{nt} \\ \epsilon_{\theta\theta} \end{Bmatrix}. \quad (10)$$

On the other hand, if the radial crack is postulated to have fully formed first, then $\sigma_{\theta\theta}$ is set to zero and the

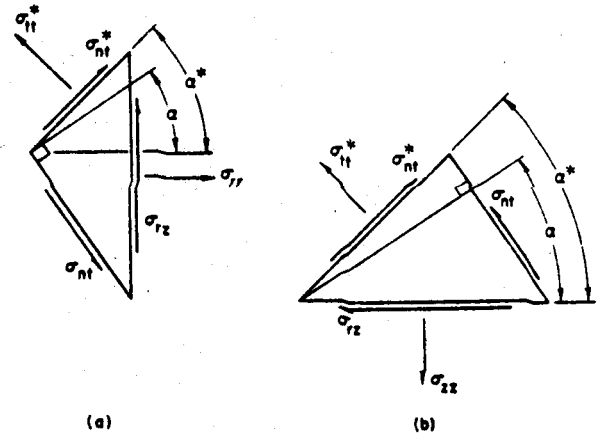

Fig. 3. Internal forces under non-orthogonal cracking.

remaining stresses become

$$\begin{Bmatrix}\sigma_{tt}\\ \sigma_{nt}\end{Bmatrix} = E\begin{bmatrix}1 & 0\\ 0 & \beta G\end{bmatrix}\begin{Bmatrix}\epsilon_{tt}\\ \epsilon_{nt}\end{Bmatrix}. \qquad (11)$$

Here again the principal stress is not σ_{tt} but is expressed by eq. (7) with the corresponding position. The resolution of stresses into the components of the $r-z$ plane is accomplished by eq. (5) where σ^*_{nn} is set to zero.

Eqs. (10) and (11) also apply to the case where a third crack has initiated and is in the process of formation. Then the last principal stress is assigned by eq. (4). If all three cracks have been fully developed in the element, all stresses are taken to be zero.

Owing to the oscillatory nature of the motion of the vessel, the cracking model must account for the possibility that a fully developed crack may close or an impending crack may be arrested if compressive loading is detected. The strain normal to each crack monitors this condition: if the strain normal to a given crack is found to be less than zero, then a fully developed crack is assumed to have closed and the development of a crack is assumed to be interrupted. The element is then able to sustain compressive loading in that particular direction. With the closing of a crack or arrest of cracking, the tensile limit normal to the crack is changed and stored for later use. If a fully developed crack closes, then the tensile limit is set to zero. However, in case the crack formation is interrupted, the stored tensile limit is assigned that particular value of stress which corresponds to the time of crack arrest. The element is hence governed by the reduced tensile limit if and when it is again reloaded in tension.

As for the inelastic behavior in compression, only the simplest and crudest possible model consisting of a maximum compressive limit on the principal stresses is considered at this stage. In compression the stress in the element may be defined by the previous expressions, depending on how many principal stresses reach the compressive limit f'_c at the same time. At the present, the maximum uniaxial stress f'_c is used as the maximum stress that the element may be able to sustain.

3.2. Reinforcement

In this analytical model the reinforcement is superimposed over the concrete element as if it were uniformly distributed over the entire element as an anisotropic material. Uniaxial reinforcement within the element can be prescribed as a percentage of reinforcement in three directions – one being the circumferential direction, and the other two positioned arbitrarily within the $r-z$ plane, as shown in fig. 4.

For purposes of computing the stresses of reinforcement in the $r-z$ plane the strain in the direction of the reinforcement must be found. If the angle between the r axis and the axis of the reinforcement is ϕ_1 or ϕ_2, the strain along the respective directions correspond to ϵ_{nn} in eq. (3). The strain in any circumferential reinforcement of the element is $\epsilon_{\theta\theta}$. Although the reinforcement typically exhibits plastic hardening, for the sake of simplicity an elastic, perfectly-plastic material behavior is assumed; this gives the following stress–strain

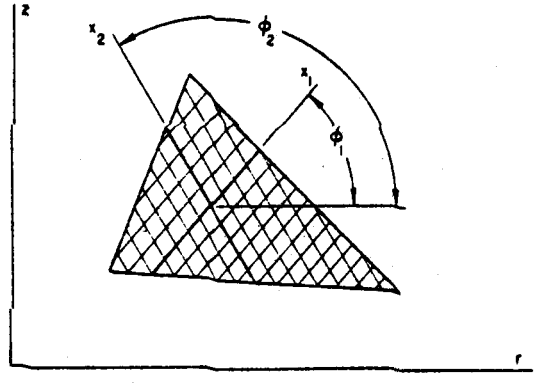

Fig. 4. Reinforcement within the $r-z$ plane.

relation

$$\Delta\sigma_s = E_s\Delta\epsilon_s\,, \quad \text{if } |\sigma_s| < \sigma_y \text{ or } \sigma_s\Delta\epsilon_s < 0$$
$$\sigma_s = \sigma_y\,\text{sign}(\Delta\epsilon_s)\,, \quad \text{if } |\sigma_s| = \sigma_y \text{ and } \sigma_s\Delta\epsilon_s \geqslant 0\,, \tag{12}$$

where the reinforcement strain is ϵ_s, its increment is $\Delta\epsilon_s$, the yield stress of the material is σ_y, and σ_s is the axial stress in the reinforcement.

The contribution of the reinforcement stress to the total element stress is then given by

$$\sigma_T = \sigma_s A_r/A_c\,, \tag{13}$$

where A_r and A_c are the cross-sectional areas of reinforcement and concrete with normals in the directions of ϕ_1 and ϕ_2, respectively. The stress in eq. (13) needs to be transformed into the cartesian components if reinforcement lies in the r–z plane; for circumferential reinforcement σ_T corresponds to $\sigma_{\theta\theta}$. Finally, the cartesian stress components due to concrete and steel are summed to obtain the overall stress in the element.

3.3. Simulation of prestressing

The prestressing is represented by layers of homogeneously distributed tendons which are modeled by thin axisymmetric shell elements (with $\nu = G = 0$ in the plane of the shell). These shell elements are superimposed over the gird of the reinforced concrete body of the PCRV and are connected through sliding interfaces so that they can stretch and slide along a predetermined path, simulating the behavior of the tendons.

Prestressing is most commonly effected by gradually loading the prestressing members up to the specified prestress load at a prescribed rate at the points where they are attached to the concrete. An equal and opposite load is also exerted on the concrete grid at these nodes so that equilibrium is maintained. When the specified prestress limit is reached, the prestressing tendons and concrete are locked together at these nodes and remain so from then on. The prestressing operation is then considered complete.

4. Comparison with experimental data

Since the analytical modeling of reinforced and prestressed concrete is rather complex, few analytical solutions are available. Furthermore, the model of the material behavior is rather crude and simplified. Therefore, an experimental corroboration must be relied upon. Several such comparisons with various model tests reported in the literature will now be given.

4.1. Internally pressurized cylindrical container

The experimental data used in this comparison pertains to an internally pressurized prestressed cylin drical container tested at the University of Illinois, Urbana [11]. This container simulates the containment of a nuclear reactor, and is shown in fig. 5. The right-hand side of fig. 5 identifies the components of the test structure, while the left-hand side shows the analytical model used in the comparison. As can be observed, no reinforcement is provided.

The concrete is characterized by a tensile limit of 3.10 MN/m^2, a compressive limit of –49.23 MN/m^2 with an initial elastic modulus of 29.7 GN/m^2 and a Poisson's ratio of 0.15. The prestress material has a modulus of 192 GN/m^2 and a yield stress of 1655

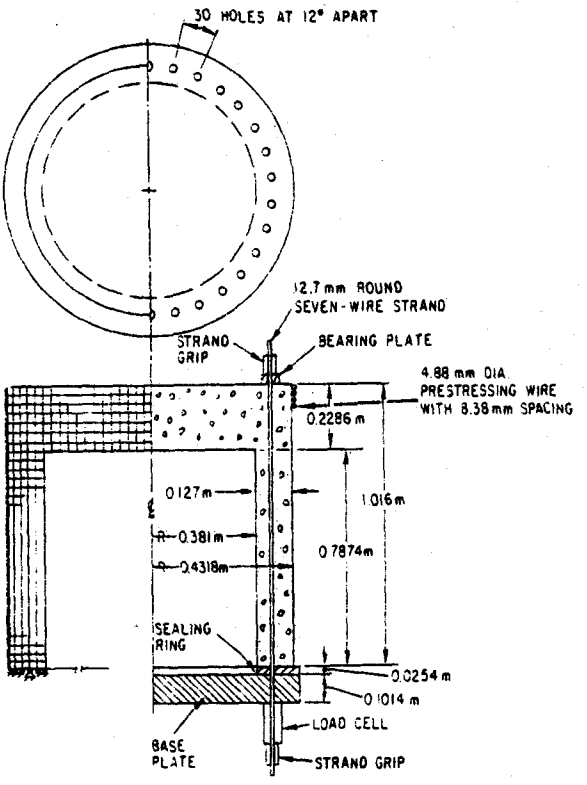

Fig. 5. Test and analytical model configurations.

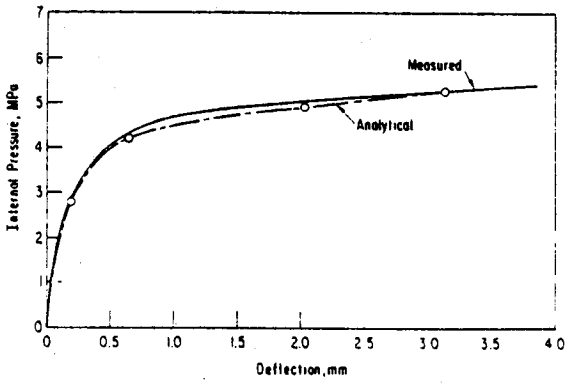

Fig. 6. Central deflection of the top cover under applied pressure.

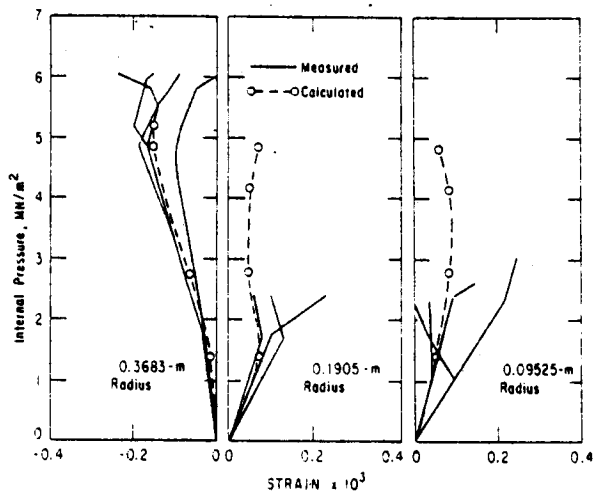

Fig. 7. Radial strain at top of the cover.

MN/m^2. Before the internal pressurization is applied, each layer of tendons is prestressed longitudinally to a force of 0.112 MN and prestressed circumferentially to an equivalent pressure of 3.52 MN/m^2.

It should be emphasized that while the experimental data pertains to static conditions, the analytical results are based on a computer code which is expressly written for dynamic problems. The use of a dynamic code for a static simulation is inefficient and rather expensive, but it nevertheless provides a good validation for the method.

The static results were thus simulated by a set of individual dynamic runs, all of which involved the same prestress loading. The pressurization in each of these runs consisted of a ramp loading to a given pressure, followed by a constant pressure at that level. Each individual run involved a different pressure level. In the first phase the pressurization proceeded at a loading rate higher than that encountered in the experiment.

The general response of the model would roughly follow the history of the pressurization coupled with the dynamic oscillation superimposed over the static value. The static equivalent response was thus estimated by visual elimination of the dynamic component from the overall results.

The analytical simulation of a static experiment by means of a dynamic code, as used in this comparison, involves certain error sources. Because of the dynamic overshoot, the analytical model would be exposed to higher stresses, resulting in additional cracks, which

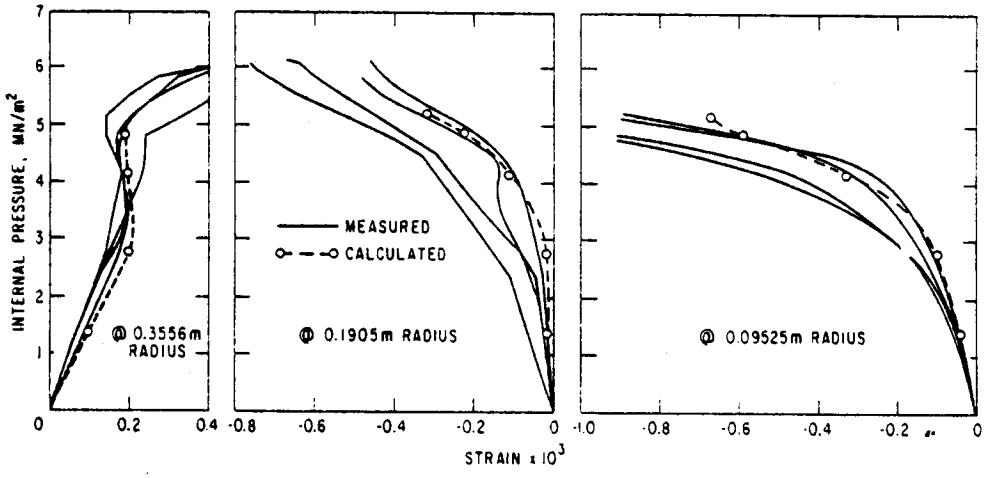

Fig. 8. Radial strain at the bottom of the cover.

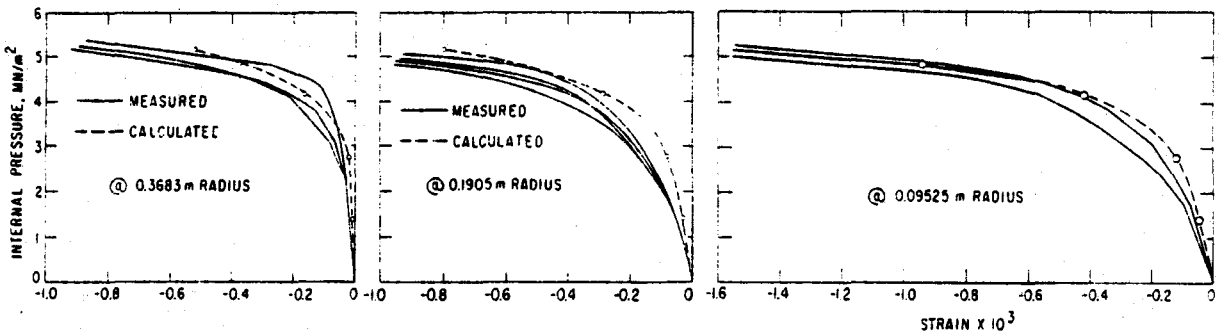

Fig. 9. Circumferential strain at the bottom of the cover.

in turn would make the material 'softer'. Thus, because of the overshoot beyond the tensile limit the model would effectively overestimate the true results.

Fig. 6 shows the central deformation of the cover with respect to internal pressure. The close agreement is encouraging since the nonlinearity of the deflection stems from the cracking in the concrete; without cracking, the deflection would be linear along the initial slope.

Figs. 7–9 show the comparison of experimental strain readings on the cover with code calculations. Fig. 7 shows the radial strain on the top surface of the cover at three radial locations. Four sets of experimental data are shown at each of the radial distances. The calculated strain falls within the experimental data.

The radial strain at the bottom of the cover is shown in fig. 8. Again, the data of four gauges, each located at the same distance from the center, is compared with the calculated results. Although sometimes at the fringes of the experimental results, the calculated values compare quite well with the measurements.

The circumferential strains at the bottom of the cover are given in fig. 9. The calculated results show a stiffer response at the low pressures. This is consistent with the elastic representation of the concrete in compression; in reality concrete exhibits softening with increasing compression. This effect seems to be offset at higher pressures by the occurrence of cracking.

The overall agreement between experiment and calculation is surprisingly good. All the results shown pertain to the cover of the model. Since the cover is not reinforced, the quality of comparisons largely reflect on the crack modeling of concrete. Based on this comparison with static results, the preliminary formulation of crack formation appears quite adequate for the treatment of concrete cracking. A comparison of experiment and analysis under dynamic conditions will be presented in subsequent sections.

4.2. Dynamically loaded beam

The experimental data referred to in this section also originated at the University of Illinois, Urbana [12]. The details of the reinforced concrete beam tested together with the supporting system are shown in fig. 10(a), while the analytical model used in the comparison is given in fig. 10(b). Fig. 11 indicates the time-history of the applied load on the beam.

Since the reinforcement is assumed to be distributed evenly throughout each of the elements, it may be characterized by averaged vertical and horizontal reinforcement densities in the interior elements. The only elements without reinforcement are located within the top and bottom layers of the beam.

The history of central deflection of the beam is shown in fig. 12, which depicts the experimental data and three sets of results pertaining to analytical predictions. One set of analytical results was taken from ref. [13] where a different reinforced concrete model had been used to simulate the reinforced beam; the remaining analytical results pertain to the present analysis.

The deflections predicted by ref. [13] and the present analysis, when based on given material properties, deviate considerably from the experiment. The maximum deflection is overestimated by almost 100%. The rather close correspondence of the two analytical results, however, shows that the modeling ingredients are quite similar. Furthermore, factors such as the

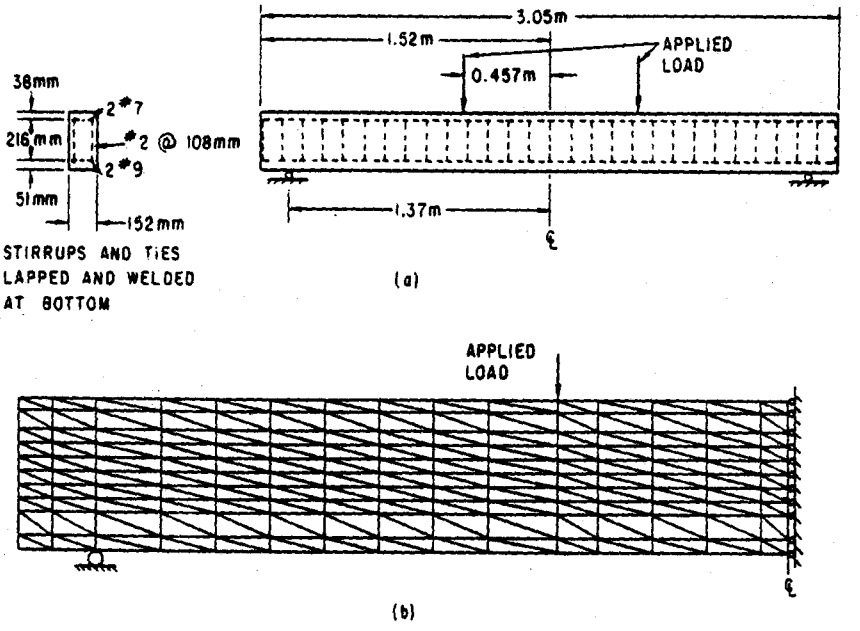

Fig. 10. Dimensions of the (a) the beam and (b) the corresponding analytical model.

bonding included in the analysis of ref. [13] are of small importance when the overall disparity with experiment data is taken into account.

The large discrepancy between experiment and analysis may be accounted for in various ways. A major part of this discrepancy is certainly due to the transient nature of the loading. The lack of accurate knowledge of the material properties is another factor. To illustrate the sensitivity of the results to the material properties, the yield point of the reinforcing steel was increased by 15%. The results are shown in fig. 12. Although such an increase is rather arbitrary, it does show the sensitivity of the results to material parameters. Another unknown under transient conditions is the crack initiation criterion. There exist other uncer-

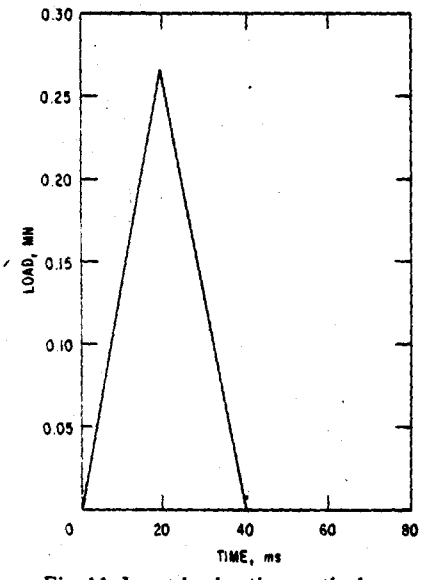

Fig. 11. Input load acting on the beam.

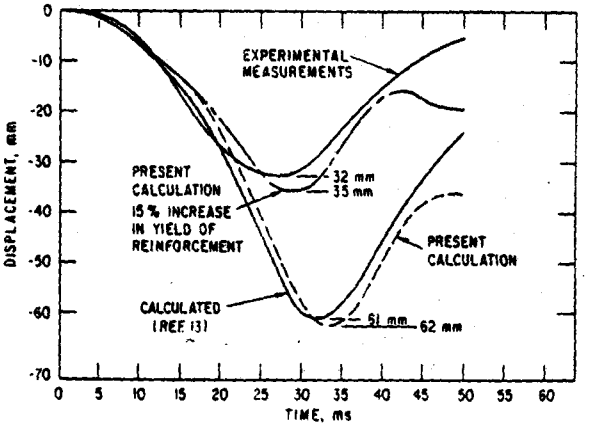

Fig. 12. Vertical deflection time history at the midplane of the beam.

tainties; they will necessitate further study in particularly designed and carefully controlled tests. Only then will accurate modeling of the problem be possible.

5. Typical PCRV structures in LMFBR design

As examples of the code's application several analytical models were analyzed to study the PCRV containment feasibility for LMFBR applications [4]. For this study the loading history was taken from another publication [14], involving conventional containment analysis of a typical 1200 MW(e) LMFBR design. A structural integrity study of the primary system had been performed using an assumed pressure–volume expansion for the core, which is shown in fig. 13. The total energy available in expanding the core to one atmosphere is estimated to be about 2720 MW-sec. The study provided a loading on the bottom of the reactor cover due to coolant impact during the core expansion. This loading was directly used for the design of an appropriate PCRV.

In the initial stage of the investigation the pressure on the top slab was assumed to be uniform, and the corresponding central plug force, obtained in a previous containment study using the REXCO code, is shown in fig. 14 for a typical pool-type reactor, and in fig. 15 for a typical loop-type reactor [14]. The pressure on the vertical walls was considered also to be uniform and half as large as that on the top slab. The inside dimensions of the PCRV models were assumed

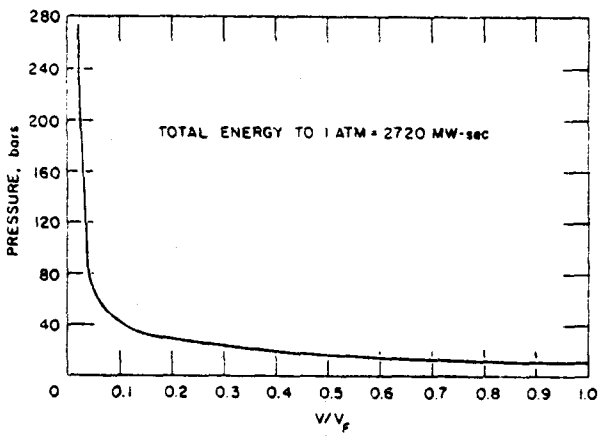

Fig. 13. Normalized core pressure–volume relationship for 4800 K average core temperature.

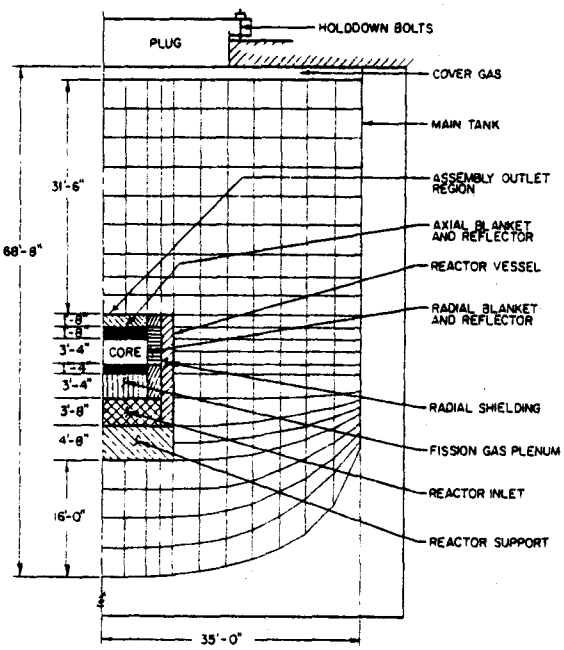

(a)

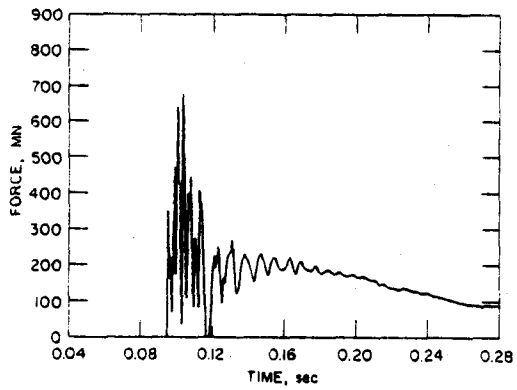

(b)

Fig. 14. REXCO model (a) and the plug force loading (b) of the pool-type reactor.

to be coincident with the outside dimensions of the REXCO models.

5.1. Conventional design of PCRVs

For the purpose of obtaining suitable preliminary dimensions and reinforcement, a simple preliminary analysis had to be carried out. First a static design was

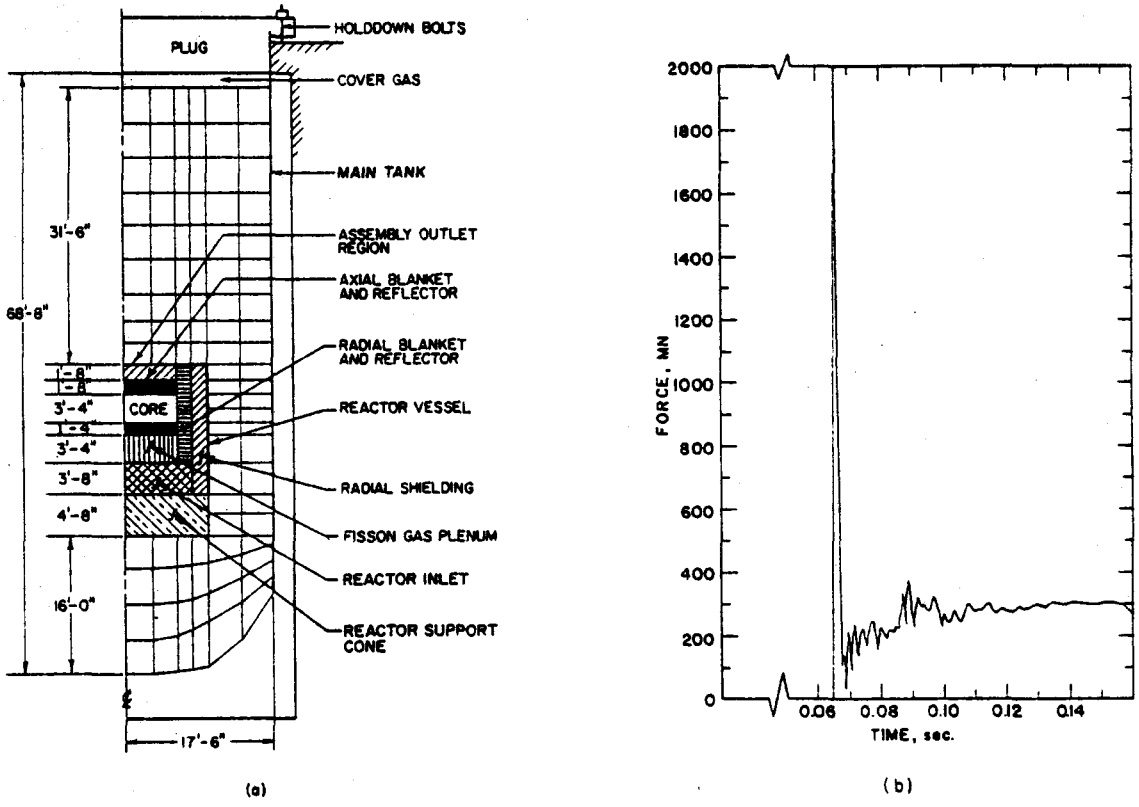

Fig. 15. REXCO model (a) and the plug force loading (b) of the loop-type reactor.

performed under the assumption that the prestressing forces should be capable of resisting internal pressures without the aid of concrete, mild reinforcement and a steel liner. The wall thickness was then determined so as to resist the prestress when acting alone. The ultimate forces in prestressing tendons, concrete and reinforcement were required to resist the assumed pressure loading with a safety factor of 1.8. The top slab was designed by considering equilibrium on a failure cone formed by 45° inclined cracks, as well as ultimate bending moment according to yield line theory. The design was checked by the empirical criterion for top slab failure, which was experimentally established at the University of Illinois, Urbana [11].

After completing the static design, the dynamic magnification factor was estimated. The fundamental vibration period of the vessel was estimated by a Rayleigh quotient using the static deflection shape due to pressure loading; this period was found to be of the same order of magnitude as the duration of the pressure peak. Therefore, the vessel was first analyzed statically for a pressure equal to the peak in fig. 14(b) (with a central plug for a peak of 680 MN). Subsequent dynamic finite element analysis showed this design to be adequate for the pool-type reactor, while for the loop-type reactor the subsequent dynamic finite element analysis indicated failure and a 30% increase of the cross sections obtained by the approximate analysis was necessary.

The PCRV designs considered in the finite element computations reported herein were based on the requirements specified in ref. [14]. These designs are shown in fig. 16 for the pool-type LMFBR, and in fig. 17 for the loop-type LMFBR. The pool vessel is provided with a 9.5 mm and the loop vessel with a 6.4 mm thick steel liner on all interior surfaces. The circumferential prestress is generated through continuous prestressed wire laid in steel-clad channels on the exterior surface. A traveling prestressing machine could be used for laying the curcumferential tendons. The top slab receives its

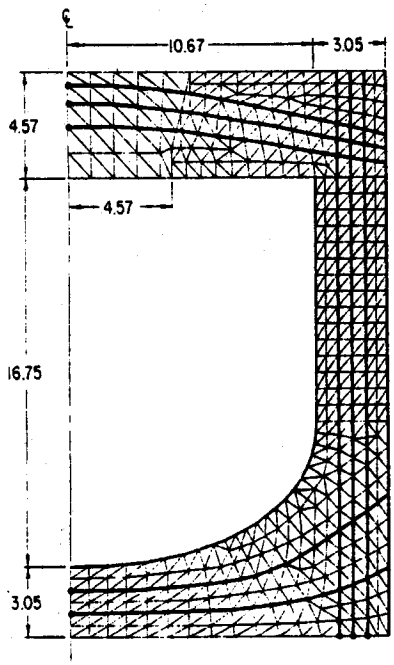

Fig. 16. Analytical model of the pool-type PCRV (dimensions in meters).

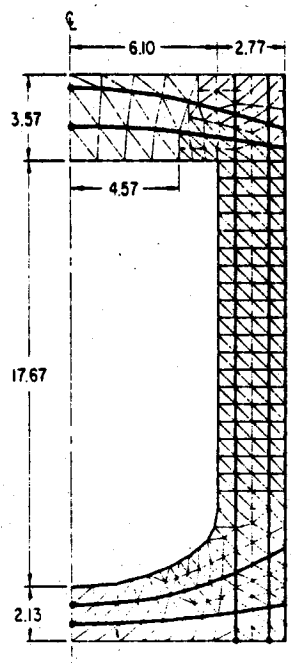

Fig. 17. Analytical model of the loop-type PCRV (dimensions in meters).

prestress partly from the circumferential wires and partly from bands of tendons crossing the top slab.

The layout of top slab tendons is made particularly difficult by the need to provide a number of penetrations in the top slab: a central plug of 9–10.6 m diameter, four penetrations of up to 2.6 m diameter for sodium pumps, eight or four penetrations of the same diameter for intermediate heat exchangers (two or one per pump), one inclined smaller penetration for the fuel handling machine, and four small penetrations required for sodium purification. These penetrations severely restrict the amount of prestressing steel that can be accommodated within the slab, although the space congestion can be alleviated by making the top slab thicker.

It is possible that, in contrast to the design considered so far, a much greater proportion of the prestress of the top slab would have to be generated by circumferential wires, reducing the number of tendons crossing the top slab or eliminating them entirely. This measure, which would help to eliminate the congestion of steel reinforcements, has no effect on service stresses; but the ultimate load behavior of the top slab, especially the ductility, would be impaired because the circumferential wires do not follow the local deformation of the top slab. Nevertheless, it would be possible to compensate for this reduction in strength by increasing the thickness of the top slab. Another alternative which might be considered is to make the top slab a composite steel–concrete structure – essentially a steel deck filled with concrete – in which full interaction between the steel and concrete and with the cylindrical walls of the PCRV is achieved by the circumferential prestressed wires as well as some prestressing tendons crossing the slab.

5.2. Results of numerical finite element computations

Having established the PCRV dimensions by approximate calculations, a dynamic computer analysis was carried out. The discretization used for the pool-type and the loop-type models are shown in figs. 16 and 17, respectively. The properties of concrete, reinforcement, and prestressing tendons, as used with the analytical model, are given in table 1. Tables 2 and 3 show the equivalent prestress load and thickness for the pool- and loop-type axisymmetric models, respectively.

The bottoms of both PCRV models were assumed

Table 1
Material properties as used in PCRV models

Concrete:		
Tensile strength	3.35	MN/m^2
Modulus of elasticity	31.7	GN/m^2
Poisson's ratio	0.18	
Density	2500	kg/m^3
Reinforcement (0.3% reinforcement in circumferential, axial, and radial directions):		
Yield point	207	MN/m^2
Modulus of elasticity	207	GN/m^2
Poisson's ratio	0.3	
Prestressing tendons (one tendon consists of 170 wires of 6.35-mm diameter):		
Wire strength	1655	MN/m^2
Modulus of elasticity	193	GN/m^2
Ultimate load of tendon	8.91	MN

to be fixed axially. Furthermore, since the primary interest in this study was the response of the main body of the PCRV, the plug was modeled only superficially. The plug was assumed to be made of material other than concrete, and therefore cracking was not permitted. The density of the plug was taken to be twice as large as that of concrete. The plug was thus designed to serve as a means of transmitting the applied load to the PCRV. To allow an axisymmetric analysis, the tendons crossing the top slab were treated as if they passed through the plug rather than around it. The plug and the top slab were thus joined by tendons (and at one additional point).

Some typical computed response results of the PCRVs are shown in figs. 18–21 for the loop-type and pool-type reactors. The period of axial vibrations was estimated to be 0.043 sec for the pool-type PCRV, and 0.028 sec for the loop-type PCRV. The respective durations of the applied pressure spikes were roughly 0.02 and 0.004 sec which is quite close to the natural period for the pool-type PCRV, but not for the loop-type PCRV. This might be the reason why the crude preliminary static analysis provided an adequate design in the case of the pool-type PCRV, but not in the case of the loop-type PCRV, so that the dimensions of the latter had to be increased by 30% to withstand the pressure pulse.

The crack configurations of maximum extent reached are shown in figs. 22 and 23. It is not unexpected that the cracks are concentrated around the corner of top slab. It is of interest to note that the pressure pulse produces some vertical circumferential cracks.

Table 2
Equivalent prestressing for pool-type PCRV model

	Radial	Axial	Circumferential
Bottom slab	$F = 26.9$ MN/m	–	$p = 5.05$ MN/m^2
	$h = 27.1$ mm	–	$h = 69.7$ mm
Top slab	$F = 17.95$ MN/m	–	$p = 5.05$ MN/m^2
	$h = 18.1$ mm	–	$h = 69.7$ mm
Cylinder	–	$F = 9.66$ MN/m	$p = 3.1$ MN/m^2
	–	$h = 9.74$ mm	$h = 42.9$ mm

Table 3
Equivalent prestressing for updated loop-type PCRV model

	Radial	Axial	Circumferential
Bottom slab	$F = 13.96$ MN/m	–	$p = 4.69$ MN/m^2
	$h = 14.1$ mm	–	$h = 41.9$ mm
Top slab	$F = 18.21$ MN/m	–	$p = 6.10$ MN/m^2
	$h = 18.3$ mm	–	$h = 54.5$ mm
Cylinder	–	$F = 10.49$ MN/m	$p = 2.77$ MN/m^2
	–	$h = 10.5$ mm	$h = 24.8$ mm

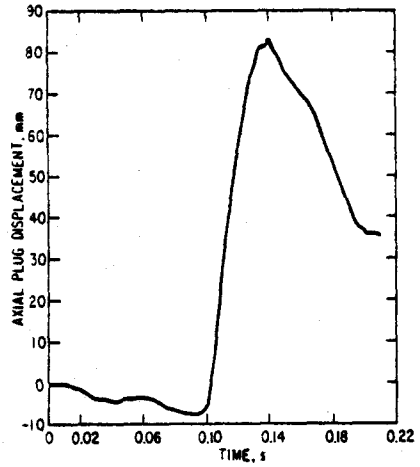

Fig. 18. Central displacement history of the plug for the pool-type model.

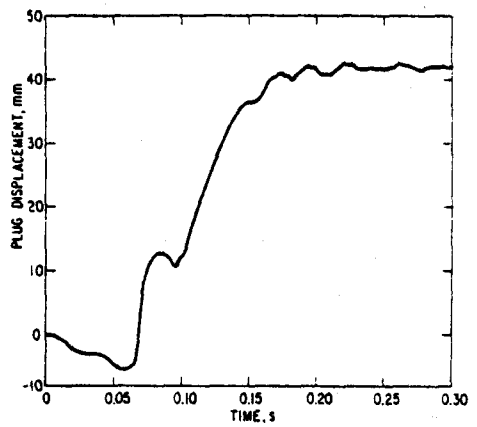

Fig. 20. Central displacement history of the plug for the loop-type model.

The fact that the displacements produced by the pressure pulse are all limited, and that the spread of cracking zones also remains limited, indicates that the PCRV designs considered are capable of resisting the pressure pulse from the HCDA. The extent of cracking found in the calculated results thus seems to be acceptable. Nevertheless, the question of maximum admissible crack opening, from the point of view of leakage limitation, should and will be further studied.

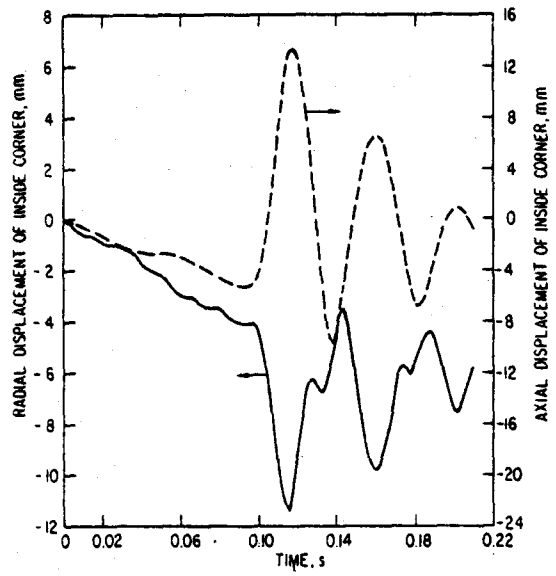

Fig. 19. Displacement history of the top inside corner of the pool-type model.

5.3. General PCRV designs

Based on the foregoing dynamic analysis and various spacial requirements, a set of preliminary general PCRV designs have been developed, both for pool-type and loop-type reactors. They are shown in figs. 24 and 25, respectively. Some differences between the analytical models and the designs shown were inevitable, due to the axisymmetric simplification as well as further changes in the designs. For example, the prestressing of the top cover in the final design of the pool-type PCRV is positioned horizontally. This was necessitated by the space restriction caused by the presence

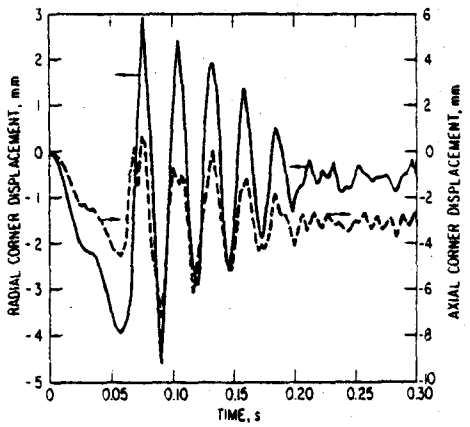

Fig. 21. Displacement history of the top inside corner of the loop-type model.

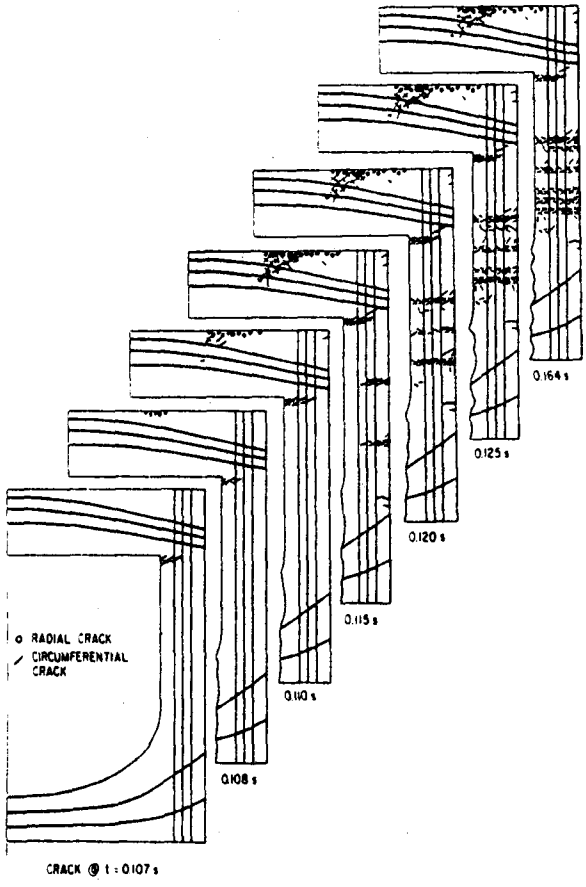

Fig. 22. Cracking sequence for the pool-type model.

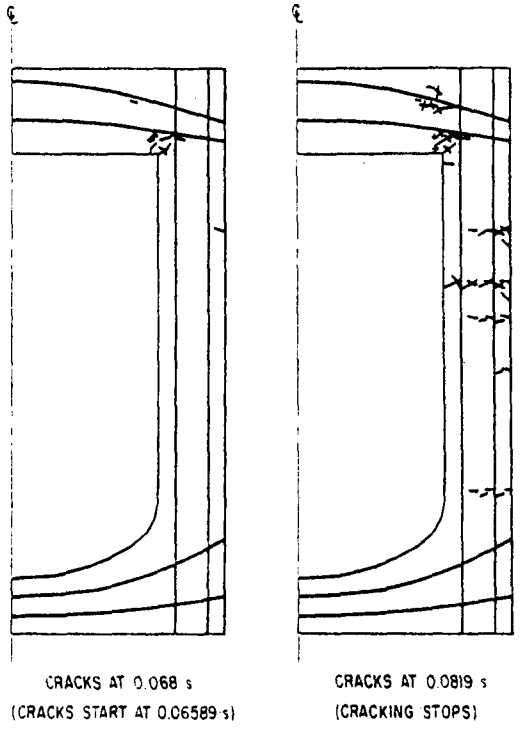

Fig. 23. Cracking sequence for the loop-type model.

of the large number of penetrations. The thickness of the top cover was also increased somewhat to improve its load-carrying capacity. Although the modified configuration has not been subjected to an analytical examination, it is sufficiently close for the design to be considered satisfactory.

According to the preliminary analysis, these designs should be able to sustain the applied load. It is also important to note that the load had been derived from an energy source that is considerably larger than the energy sources utilized in the currently prevailing safety evaluation of an LMFBR.

6. Discussion of results

The simple reinforced concrete formulation described in this paper appears to be a valuable tool to study the transient response of the PCRVs. The computer code provides a means to locate critical areas of the particular design. Parameter or sensitivity studies can also be made with great efficiency. As a matter of interest, this preliminary version is also quite efficient: one element time step takes about 0.7 msec on the IBM 370/195.

The static experimental results described in the report indicate reasonable correspondence with analytical calculations. However, the use of the present formulation to model static problems is inefficient and also expensive. The transient test results show considerable variation with analysis. Although a variation in the yield point of the reinforcing steel, as indicated before, could bring about closer agreement, the discrepancy cannot be dismissed that lightly. This is borne out by the fact that analytical models quite similar to that shown in the text produce results which vary considerably. This is a clear indication that the

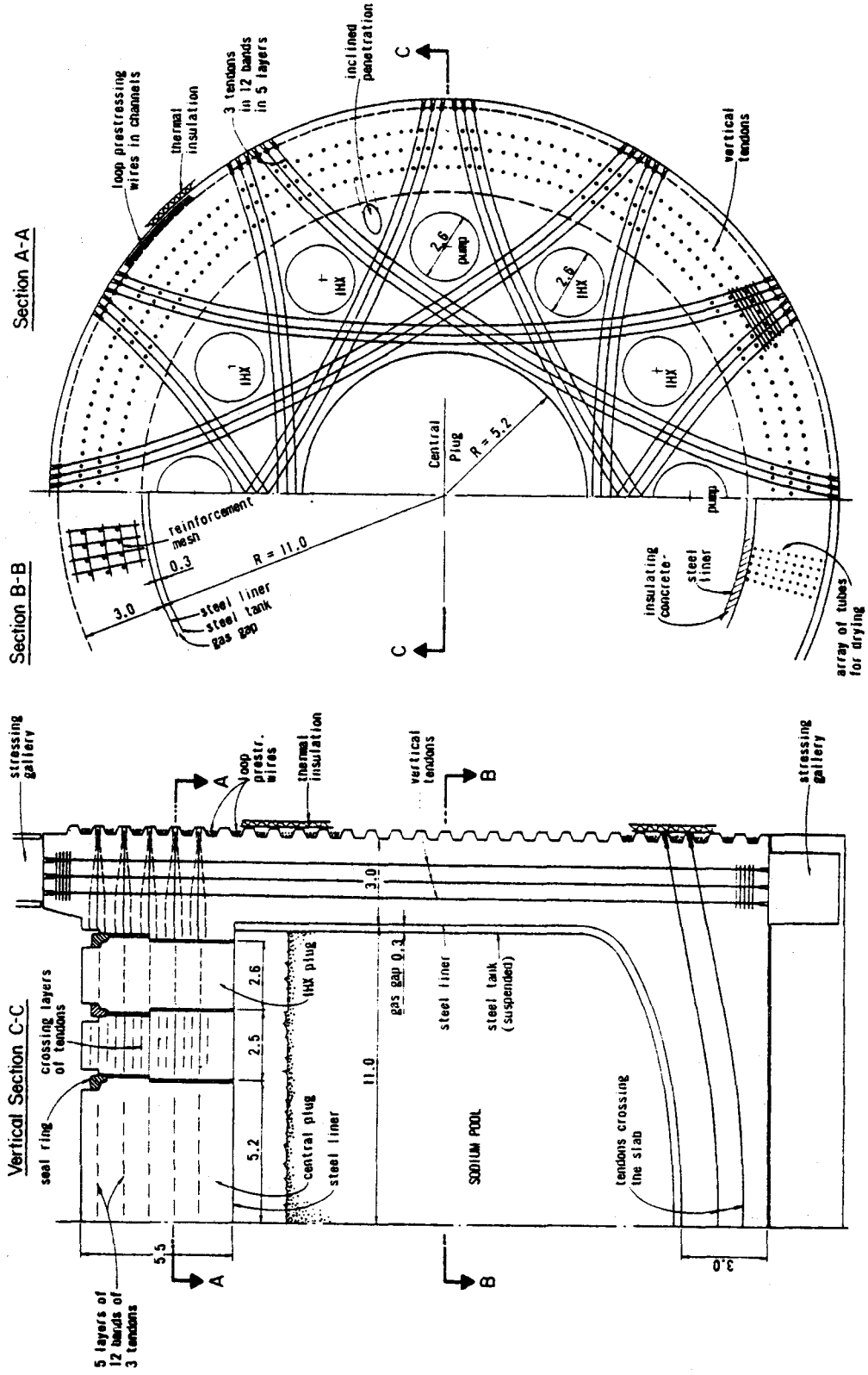

Fig. 24. General design of the pool-type PCRV (dimensions in meters).

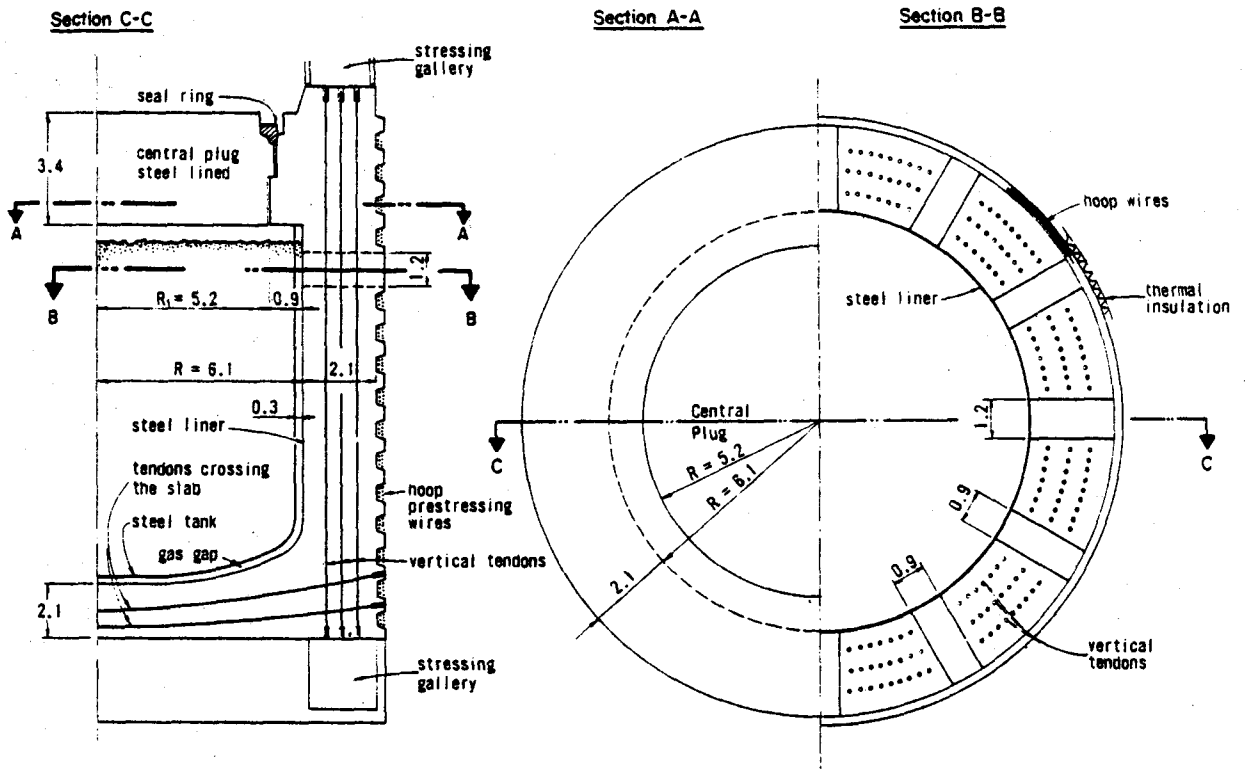

Fig. 25. General design of the loop-type PCRV (dimensions in meters).

analysis of cracking media, especially one involving transient response, is by no means as simple as it may appear initially.

Several simplifications and uncertainties could contribute to the observed discrepancies: the properties of concrete under dynamic conditions are not well known; the crack initiation based on maximum principal stress may not be a representative criterion; and neglecting strain rate sensitivity and strain hardening in the reinforcement may not be appropriate, particularly in view of the large change in results of the second example when the yield stress was increased.

It is believed that for transient analysis of cracking media, as is the case in this paper, the suppression of the computationally artificial 'crack-shock' is of great importance. A rather simple technique is used here which should be subjected to experimental scrutiny.

It is quite obvious that with the present criterion of crack initiation, the results will depend on the refinement of the discretization. From the continuum point of view the size of the elements should be systematically reduced to achieve convergence to the true answer. Yet the assumption of the reinforcement being uniformly distributed through the element requires that the elements be large in comparison with the 'density' of the reinforcement so that this assumption be valid. The two competing and opposing requirements necessarily make the modeling of a PCRV rather difficult. A compromise by analytical means is difficult to make, and parametric evaluation must be relied upon.

Keeping in mind the simplicity and preliminary stage of development of reinforced concrete model described in this paper, the results derived must be weighed with a degree of uncertainty. There are, however, trends that can be observed from the studies. For example, it is quite obvious from the results that no apparent difficulties exist in providing sufficient containment capability for even a rather large energy source as the one considered in this paper. In fact, the containment capability may well be increased with the conventional size PCRVs.

7. Conclusions

(1) Preliminary finite element results indicate that a PCRV is capable of resisting very high pressure pulses due to a HCDA. However, more accurate analyses will have to be carried out to examine local effects in complete 3D geometries, to examine the subsequent stage of theat exposure of the PCRV, post-accident heat removal, and eventual contact of concrete with sodium.

(2) Crude static analyses appear to yield a reasonable preliminary estimate of PCRV dimensions and reinforcement.

(3) The explicit finite element code formulation is suitable for the analysis of a PCRV subject to a HCDA and makes possible economical computations; even the introduction of prestress can be handled by the explicit finite element code, though this is somewhat troublesome and time-consuming.

(4) Modeling reinforced concrete in dynamic problems involving an explicit time integration, tensile cracks must be considered to form gradually rather than instantly; otherwise the spurious waves generated by sudden crack formation in the analytical model would cause a premature prediction for disintegration of the structure.

(5) It has been shown that it is possible to develop realistic designs for both pool- and loop-type PCRVs which are capable of sustaining HCDA loads.

Acknowledgement

This work is part of the Engineering Mechanics Program of the Reactor Analysis and Safety Division, Argonne National Laboratory and it was supported by the US Department of Energy.

References

[1] S.H. Fistedis, Nucl. Eng. Des. 3 (1966) 281.
[2] Z.P. Bažant, Nucl. Technol. 30 (1976) 256.
[3] Z.P. Bažant and S.H. Fistedis, Nucl. Eng. Des., to be published.
[4] A.H. Marchertas et al., Trans. 4th SMiRT Conf., San Francisco (1977), Paper E4/1.
[5] Y.W. Chang and J. Gvildys, Argonne National Laboratory Report, ANL-75-19, June (1975).
[6] Chung-Yi Wang, Argonne National Laboratory Report, ANL-75-81, Dec. (1975).
[7] Chung-Yi Wang, in: Proc. 12th Annual Meeting Society of Engineering Scientists (University of Texas, Austin, 1975) p. 919.
[8] T.B. Belytschko and B.J. Hsieh, Int. J. Numer. Methods Eng. 7 (1973) 255.
[9] L. Seaman et al., Poulter Laboratory Technical Report 003-76, SRI, June (1976).
[10] M. Suidan and W.C. Schnobrich, J. Struct. Div., ASCE 99 (ST10) (1973) 2109.
[11] S.L. Paul et al., University of Illinois Civil Engineering Studies, Structural Research Series No. 346, Urbana (1969).
[12] A. Feldman et al., University of Illinois, Report No. DASA-1259, D74-174, Urbana (1962).
[13] S. Adham et al., AFWL-RE-74-22, Feb. (1975).
[14] A. Amarosi et al., Argonne National Laboratory Report, ANL-76-61, May (1976).